Build-up strategies for additive manufacturing of three dimensional Ti-6Al-4V-parts produced by laser metal deposition

Cite as: J. Laser Appl. **30**, 022001 (2018); https://doi.org/10.2351/1.4997852
Submitted: 27 July 2017 . Accepted: 05 March 2018 . Published Online: 23 March 2018

Felix Spranger, Benjamin Graf, Michael Schuch, Kai Hilgenberg, and Michael Rethmeier

Build-up strategies for additive manufacturing of three dimensional Ti-6Al-4V-parts produced by laser metal deposition

Felix Spranger,[1] Benjamin Graf,[2] Michael Schuch,[3] Kai Hilgenberg,[1,4] and Michael Rethmeier[1,2,4]
[1]*Federal Institute for Materials Research and Testing, Unter den Eichen 87, 12205 Berlin, Germany*
[2]*Fraunhofer Institute for Production Systems and Design Technology, Pascalstraße 8-9, 10587 Berlin, Germany*
[3]*Bundeswehr Research Institute for Materials, Fuels and Lubricants (WIWeB), Institutsweg 1, 85435 Erding, Germany*
[4]*Institute for Machine Tools and Factory Management, Technical University Berlin, Pascalstraße 8-9, 10587, Berlin, Germany*

(Received 27 July 2017; accepted for publication 5 March 2018; published 23 March 2018)

Laser metal deposition (LMD) has been applied as a coating technology for many years. Today, the technologies capacity to produce 3D depositions leads to a new field of application as additive manufacturing method. In this paper, 3D laser metal deposition of titanium alloy Ti-6Al-4 V is studied with special regard to the demands of additive manufacturing. Therefore, only the coaxial LMD powder nozzle is used to create the shielding gas atmosphere, which ensures high geometric flexibility. Furthermore, specimen with high aspect ratio and hundreds of layers are manufactured, which represent typical features in additive manufacturing. The presented study contains the following steps: First, cylindrical specimens are manufactured with a standard shell-core build-up strategy and mechanical properties as well as fracture mechanisms are determined. Based on the results, experiments are conducted to improve the build-up strategy and new tensile test specimens are built with the improved strategy. The improved strategy incorporates variable track overlap ratios to achieve a constant growth in the shell and core area. As blanks, lean cylinders comprising more than 240 layers and a height of more than 120 mm are manufactured. The specimens are analyzed by X-ray inspection for material defects. Fractured surfaces are observed via scanning electron microscopy and the composition of the surfaces is determined using energy dispersive X-ray spectroscopy. The tensile test results prove mechanical properties close to ASTM F1108 specification for wrought material. https://doi.org/10.2351/1.4997852

Key words: laser metal deposition, additive manufacturing, Ti-6Al-4V, Ti64, titanium alloy, aircraft components, turbine components, build-up strategy, mechanical properties

I. INTRODUCTION

According to the current aviation program "Flightpath 2050—Europe's Vision for Aviation" the number of commercial flights within Europe will increase from 9.4 million in 2011 up to 25 million in 2050.[1] In addition, the fuel consumption as well as the CO_2 and NO_x emissions must be reduced up to 75% and 65%, respectively.[2] To reach these ambitious goals, materials with a high specific strength have to be used in aerospace components. Excellent mechanical properties (e.g., low and high temperature strength) and good corrosion resistance in combination with low density make titanium alloys to a favorite material for these purposes. For instance, in a Boeing 777 aircraft almost every metallic part of the landing gear consists of titanium alloys. Besides Ni-based alloys, this class of materials is the most common material for blades and other heat stressed parts. It should be also noted that up to 7% of an Airbus A330 as well as A340 is made of titanium alloys.[3]

However, high performance Ti-alloys are typically "hard-to-machine" materials and expensive in comparison to Fe-, Al-, or Mg-based alloys.[4] Therefore, reliable manufacturing and repair technologies have to be developed in order to reduce the component costs. One approach is the use of additive manufacturing technologies like selective laser melting, electron beam melting or laser metal deposition (LMD) to build up complex and near net shaped components. The later one is characterized by several challenges which have to been resolved.

In particular, Ti-alloys are susceptible to the reaction with atmospheric gases in the liquid as well as in the solid state. If the surface temperature increases above 300 °C, a diffusion of oxygen, nitrogen, or hydrogen leads to an embrittlement of the material.[5] Therefore, the demands regarding to the shielding gas atmosphere are high. Several investigations like Refs. 6 or 7 show that this issue becomes more serious when parts with small base areas or volumes like lean pillars, single track walls, or thin walled turbine blades are build-up. As layers are consecutively deposited on top of each other they act gradually as a barrier for the heat conduction to the substrate. This leads to a rising heat accumulation, larger heated areas and prolonged cooling times. Consequently, the formation of a strong heat tint, indicating a severe oxidation, is more likely.[6,7] So far, there are three different approaches to deal with this issue.

- Additional shielding gas nozzles: Trailing gas nozzles are applied in fusion welding. For additive manufacturing with LMD, an additional ring nozzle can be applied to improve the size of the shielding gas atmosphere,[8] although it limits the geometric flexibility of the powder nozzle.
- Process chamber: Experiments with LMD in an argon flooded box are shown in Ref. 9, where atmospheric gases are displaced with a constant flow of argon. Wang applies this process chamber in Ref. 10 for LMD of Ti-6Al-4 V. The deposition of large structures is described in Ref. 11. Besides the high argon consumption, the box limits the specimen size and impedes movement and inclination of the powder nozzle. It is therefore difficult to adjust the build-up strategy for different 3D structures.
- Material deposition close to a substrate plate: A thick substrate plate provides good heat dissipation. This leads to shorter cooling periods and reduced requirements for the shielding gas atmosphere. Tensile test results with this strategy are given by Yu in Ref. 12. The dynamic behavior of specimen deposited close to the substrate with a height of 5 mm is described in Ref. 13. Material deposition is not representative for additive manufacturing with LMD, where it is necessary to deal with heat accumulation during the build-up of 3D-structures, and a variation of different heat dissipation conditions.

The described methods work well in their respective applications, although they are not able to comply with all demands of an additive LMD process. For additive deposition on components with complex shape and for the adjustment of build-up strategies, a high spatial flexibility for the powder nozzle is essential. The LMD nozzle fulfils these demands, although issues with the restricted size and quality of the local shielding gas atmosphere lead to challenging manufacturing conditions for Ti-alloys. The feasibility and limitations of this method are discussed in this paper.

II. STATE OF THE ART

Originally, LMD was developed to produce coatings on metallic substrates using powder or wire materials. Due to high deposition rates, large working areas, and low porosity material deposition, LMD gained more and more attention in the industrial application for additive manufacturing purposes.[14] Candel-Ruiz *et al*. discuss in Ref. 15 the feasibility of LMD to produce additional features on existing components, like 3D reinforcements. Furthermore, the technology's capability to combine multiple materials is shown. In Ref. 16, Wu *et al*. describe the manufacturing of various Ti-6Al-4 V components, for example, tubes with rectangular shape. LMD as additive technology for aerospace and automotive applications is discussed by Hedges and Calder in Ref. 17.

LMD as repair technology for components made of titanium alloys is described in Ref. 18, where milled grooves are filled with new material for crack repair purposes. For additive manufacturing of complex geometries, limitations of the process regarding dimensional accuracy and inconsistent material properties need to be dealt with.[19,20] Furthermore, if laser metal deposition is used to produce aviation components, great effort has to be put into qualification, testing and certification of additive manufactured parts and the fabrication process itself.[4]

The LMD-process is illustrated in Fig. 1. Powdery material is blown into a molten pool which is created on the surface of the substrate by a laser beam. The powder is carried by an inert gas stream and solidification takes place in a local inert gas atmosphere. The complex sub processes and process variables corresponding to the physical stages of the deposition are described in Ref. 21.

A. 3D-build-up and macrostructure

The smallest design element in the LMD-additive manufacturing processes is a single weld bead. Main process parameters influencing the bead height or width are the laser power, the welding velocity, the powder mass flow, and the beam spot diameter.[22] Adjoining single beads with a defined overlapping factor form single "two-dimensional" layers. Zhang *et al*.[23] found that the overlapping factor or stepover itself is an important element to adjust the layer height. An increasing overlapping factor leads to an increased height of the layer, while the layer height decreases with a decreased track overlap. Hence, to get an even surface, which is desirable for a constant build-up process, the overlapping factor needs to be continuous. Otherwise, if three dimensional parts are built by a variety of superimposed layers, already small differences in overlapping factor can lead to a discrepancy of the height within the layers due to systematic error propagation effects.[24,25]

Even if the single layer height is uniform due to the application of a constant overlapping factor, the superimposition of simple pendulum deposition paths leads seldom to a high dimensional accuracy over a variety of layers. Deviations in the build-up process are mainly caused by heat accumulation effects during the process and/or inadequate tool path trajectories or parameters.[19] Especially lower deposition rates near edges have to be taken into account when perpendicular walls are required.[26] Therefore, in many publications different build-up strategies were investigated and developed to enable the additive manufacturing of specific near net shape geometries. Montero *et al*. investigated in Ref. 19 strategies to build-up blocks with perpendicular edges. Like in Ref. 25, a shell-core strategy turned out to be best applicable to obtain near net shaped parts. In both applications, lower deposition rates along the contour were compensated by multiple shell-deposition paths. To fabricate lean cylinders ($d = 19$ mm, $h = 120$ mm) with perpendicular

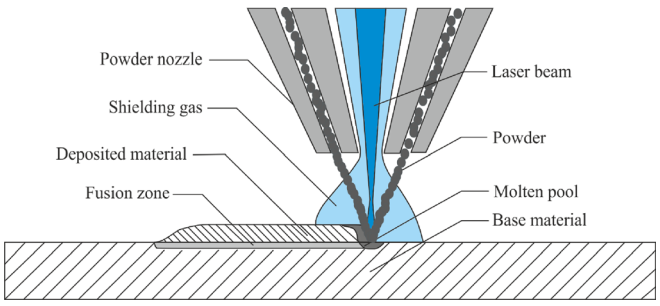

FIG. 1. Schematic process view and layer composition.

edges, Petrat *et al*. applied two superimposed circles per layer to build-up the near net shape shell. Furthermore, the core of the cylinders is filled by a pendulum strategy.[25] This approach offers some important advantages compared to a circle or spiral strategy as investigated by Zhang *et al*.[27] Circles with small diameters require high accelerations of the machines axes which can affect the accuracy of the movement. Moreover, prolonged deposition times in the inner cylinder areas can cause a heat accumulation. Nevertheless, the advantages of the applied shell-core strategy, geometrical imperfections, that made regular checks necessary, occurred in appearance of a negative hemisphere profile in the middle of the pendulum area. Therefore, the build-up strategy utilized in Ref. 25 was divided into a standard layer with constant track overlaps (as possible) and a compensation layer, see Fig. 2. After every eight standard layers, a decrease of the middle area requires a compensation layer consisting of a small square in the inner field. The resulting top has an even surface again. Additionally, a constant rotation of the starting point to compensate different deposition rates was applied.

For 3D-build-up with LMD, the multiple deposition of single layers on top of each other leads to thermal cycles in the material. These thermal cycles are influenced by the substrate temperature and the capability for heat deduction. Zhang[28] studies the influence of substrate preheating with a finite element model to calculate the thermal flow from the process zone, through the deposited material and to the substrate. Based on numerical simulation and experimental investigation, Zhang describes the influence of preheating temperature on microstructure, hardness and mechanical properties. Zhang considers the preheating temperature a major influence on the 3D-build-up of thin wall structures. A numerical model for the build-up process is presented in Ref. 29 by Peyre. The thermal cycles are simulated with a finite element model. The results show that for thin-walled structures the heat deduction changes with increasing height of the structure. Therefore, the size of the molten pool changes, and the dimensions of single weld beads are influenced.

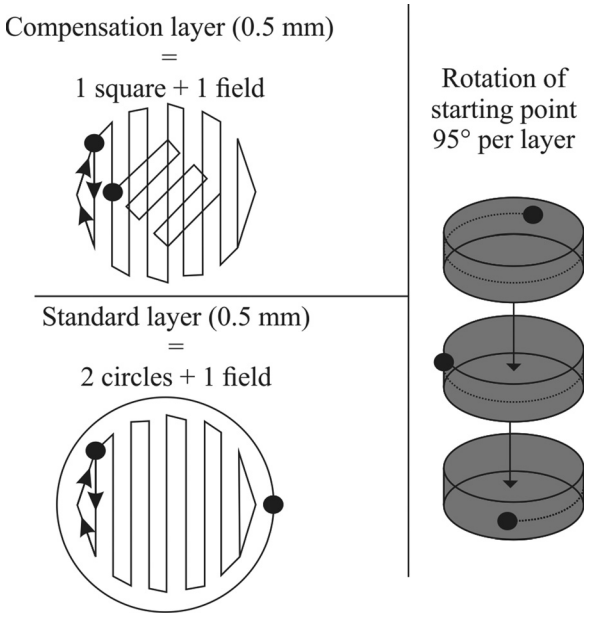

FIG. 2. Build-up strategy developed by Petrat *et al*. (Ref. 17).

One option to deal with the issue of changing heat deduction is the application of process monitoring and control. The goal is the adjustment of process parameters inline in order to achieve a constant material deposition. Different monitoring technologies are studied in the literature, including pyrometry and IR cameras.[30] Tang and Landers show in Ref. 31 that information about the melt pool temperature alone is not sufficient for a control system to achieve uniform track dimensions. Different sizes of melt pools can have the same temperature profile. Therefore, a full control system needs to take further information into account. Mazumder *et al*. present a hybrid monitoring system, which combines pyrometer based temperature measurement with three high-speed CCD cameras.[32] The corresponding hybrid process controller is able to achieve a constant layer height. Mazumder demonstrates the feasibility of this setup with the additive build-up of a complex turbine blade, where the controller leads to a greatly improved dimensional accuracy.

B. Shielding gas protection and microstructure

Besides the potential to manufacture complex 3D macrostructures, the deposition process offers unique opportunities to manipulate the microstructure as well. According to findings by Wu,[33] the microstructure of LMD fabricated components differs substantially from conventional material due to the high cooling rate (10^6 K/min) of the molten material. By the use of adequate process parameters, fine-grained microstructures with columnar shape can lead to similar or even superior mechanical properties in comparison to wrought or casted Ti-6Al-4 V components.[33] But, during the 3D build-up process, different effects like heat accumulation or inadequate shielding gas conditions can lead to a coarsening of the microstructure and to material embrittlement. It is essential to achieve sufficient shielding gas coverage and understand the thermal conditions during metal deposition.

C. Mechanical properties of Ti-6Al-4 V for additive LMD

The literature contains studies of mechanical properties via tensile tests. Oftentimes flat tensile specimens are manufactured. These specimens are extracted of simple additive manufactured walls, cubes or few single layer welds. In a minority of cases near net shaped specimens are fabricated directly. Mostly, to avoid issues with shielding gas atmosphere, they are built in argon flooded boxes[34,35] and are extracted in favorable directions (across the build-up direction). Afterward, they receive a heat treatment or hot isostatic pressing. In these studies, the tensile strength can reach values of cast material[36–40] and in some cases the properties exceed those of forged specimen. The elongation at fracture is mostly comparably low (<10%). Overall, it is shown within these tensile tests that LMD is applicable for the additive manufacturing in argon gas protection chambers. A summary of mechanical properties is given in Table I.

These studies do not embody additive manufactured components or geometries with high aspect ratios like turbine components, which consist of more than hundred

TABLE I. Mechanical properties of Ti-6Al-4 V, specification and literature values.

Material condition	Ref.	Yield strength in MPa	Tensile strength in MPa	Elongation in %
Cast material	ASTM F1108 specification	>758	> 860	> 8
Wrought material	ASTM F1472 specification	>860	> 930	> 10
LMD as deposited, in process chamber	Beese *et al*. (Ref. 40)	960 ± 26	1063 ± 20	10.9 ± 1.4
LMD in build-up direction and HIP'ed	Kobryn *et al*. (Ref. 38)	899	1002	11.8
LMD, flat specimen	Yu *et al*. (Ref. 12)	976 ± 24	1099 ± 2	4.9 ± 0.1

superimposed layers. Such components cannot be built with their main axis flat on the substrate. Components with high aspect ratio are susceptible for heat accumulation and for consequences like material embrittlement and grain coarsening effects. Instead of flat tensile specimen, upright cylinders provide a much better representation of these kind of geometries. To fabricate suitable blanks, the limitations of the LMD process need to be dealt with by developing appropriate build-up strategies. Moreover, suitable and cost-efficient deposition conditions are needed to process Ti-6Al-4 V adequately.

III. EXPERIMENT

The experiments are conducted using a TRUMPF TruDisk 2.0 kW Yb:YAG Laser and a 3-jet powder nozzle. The carrier gas for powder transportation is Helium with a flow rate of 4 l/min. The choice of helium as carrier gas is according to manufacturer specification. Due to the low density of helium, the turbulent flow induced by the carrier gas is reduced, and the laminar shielding gas flow is not disturbed. Argon with a flow rate of 10 l/min is applied as shielding gas. The gases feature a purity ≥99.999%. The Ti-6Al-4 V substrate features a thickness of 25 mm. The chemical composition of the 45 μm–105 μm grain sized powder material is given in Table II.

A. Cylinder build-up with basic deposition strategy and compensation layers

A cylindrical specimen geometry is chosen because this geometry is well suited to study issues with heat accumulation. Compared to its height, the contact area to the substrate plate is small, therefore heat deduction in the substrate plate is limited. In the experimental series 1 (E1), cylinders with a height of 120 mm and a constant diameter of 19 mm are built according to the strategies presented in Ref. 25. Standard layers and compensation layers are deposited in the described and shown sequence (Fig. 2). The laser power is synchronized with the travel speed by the machine control. Therefore, a constant energy input per unit length is achieved even at turning points, where the acceleration of the machine axes leads to a slight variation in the travel speed. Processing parameters are listed in Table III.

Sixteen cylinders are built up at the same time. After one layer is deposited for a single cylinder, the laser beam is switched off and the powder nozzle moves to the starting point for the next cylinder. When one layer is deposited for every cylinder, the deposition process is continued on the first cylinder. This strategy leads to a break of approximately 7 min between the deposition of two superimposed layers for a single cylinder. This interlayer time includes the deposition and travel time for 15 cylinders. No additional shielding gas delay is applied at the specific endpoints.

The 120 mm high blanks are separated from the substrate via wire electrical discharge machining afterward. The oxygen and nitrogen content is determined along the build-up direction to evaluate the efficiency of the local shielding gas atmosphere created by the powder nozzle. Eleven disks are cut of the cylinders with a thickness of 8 mm for gas phase extraction. In a second step, round tensile specimens according to DIN 50125 are tested. The tensile specimens are machined of the upper 90 mm of the blanks, to avoid the influence of changing heat dissipation near the substrate and porosity along the shell. The fracture surfaces are examined via scanning electron microscopy (SEM) and the composition of the surfaces is determined via energy dispersive X-ray spectroscopy (EDX).

TABLE II. Chemical composition Ti-6Al-4 V powder, above: nominal value according to ASTM B861, below: Melt analysis.

	Chemical composition in wt.%			
	N	C	H	Fe
Nominal value	Max. 0.05	Max. 0.08	Max. 0.0125	Max. 0.40
Measured value	0.005	0.005	0.003	0.19
	O	Al	V	Ti
Nominal value	Max. 0.20	5.5–6.75	3.5–4.5	Bal.
Measured value	0.12	6.40	4.06	Bal.

B. Improved build-up strategies

The experimental series for improving the build-up strategy are summarized in Table IV and described in Subsections III B 1–III B 3 in detail.

1. Avoiding compensation layers with adjusted travel paths and determination of the sag origin in E1

In experimental series 2 (E2), the cause of the geometric error in the middle of the pendulum area, recognizable as

TABLE III. LMD standard process parameters.

	Laser power P in W	Spot diameter d in mm	Welding velocity v in m/min	Powder mass flow $\dot{m}$ in g/min
Welding parameters	1000	1.0	1.0	3.75

TABLE IV. Overview of the experimental series.

Experimental series	Aim	Improvement Approach
E1	Evaluation of standard strategy	-
E2	Determination of the sag origin	Adjoining lines
E3/E4	Avoidance of compensation layers	Pendulum strategy with variable track overlap
E5a/E5b	Constant cooling conditions	Adjustment of the interlayer cooling period
E5c	Improvement of the local shielding gas protection	Adjustment of the gas delay times at endpoints

negative hemisphere profile and referred hereinafter as "sag," will be determined. Therefore, the pendulum strategy used in E1 is replaced by adjoining lines to fill the core of the cylinders. By the use of adjoining lines instead of the common pendulum strategy no turning points will occur at the transition area to the shell circles. Therefore, it is possible to determine the contribution of multiple track overlaps (in the case of the applied pendulum strategies) to the sag formation.

The adjusted travel path of the nozzle is illustrated in Fig. 3. The strategy E2 is applied for 16 layers on each of the four test cylinders. A deposition takes place only along the solid lines by activating the laser beam. The overlap ratio of the weld paths is still 50% (Table V).

2. Avoiding compensation layers with variable track overlap

To avoid compensation layers but maintain the basic pendulum strategy, a new approach is tested. Variable track overlap ratios are applied within one pendulum layer to compensate the lower deposition rates in the middle of the cylinders. Two configurations of variable track overlaps are presented in the experimental series 3 and 4, Fig. 4.

3. Optimization of the cooling conditions

In this step, appropriate cooling conditions are determined for an automatized build-up process. The cylinder

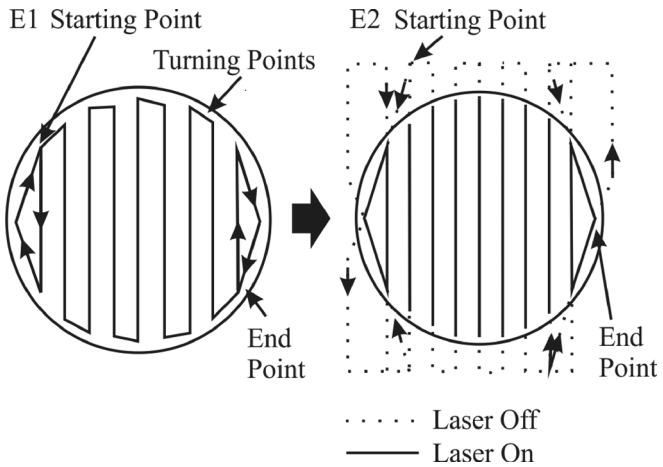

FIG. 3. Comparison of standard travel paths (E1) and travel paths using adjoining single lines to avoid turning points within the cylinder contour (E2).

TABLE V. Overview of the Experimental series E5.

Experimental series	Experimental details
E5a	Material deposition at different cylinder heights (0, 3, 15 mm) to evaluate the influence on heat dissipation
E5b	Deposition with different interlayer cooling periods (17.5, 62.5, 126 s) at 100 mm cylinder height
E5c	Determination of appropriate gas delay times till no heat tint is observable at endpoints of the pendulum area (at 126 s interlayer cooling period)

height, the interlayer cooling periods between the depositions of two superimposed layers and the gas delay times at pendulum endpoints are varied. For all the following experiments, standard layers with the pendulum strategy presented in E4 are used. The experimental series E5 include the following (Table V):

Additionally, the cooling behavior is investigated with a two-color pyrometer and thermographic camera measurements. The pyrometer measurements are conducted on the deposition endpoint of the pendulum area. The thermographic camera measurements cover the whole surface area. For the temperature measurement, up to three overlying layers are deposited on the substrate plate as well as on a cylinder with around 100 mm height.

C. Cylinder build-up with variable track overlap ratios and optimized cooling conditions

To evaluate the new build-up strategies, five cylinders are manufactured based on the results of the previous experiments. The pendulum strategy shown in E4 is applied. For the parallel build-up of five cylinders, the interlayer cooling period t_c is 126 s due to the deposition time on n-1 cylinders, the travel time, and the gas delay time as well. The latter one

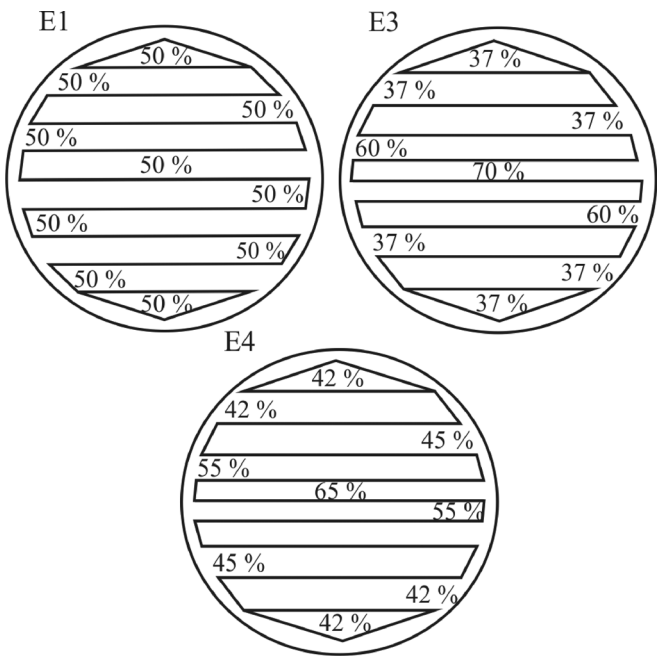

FIG. 4. Comparison of the pendulum strategies: E1 Standard strategy; E3, E4 strategies with variable track overlap ratios.

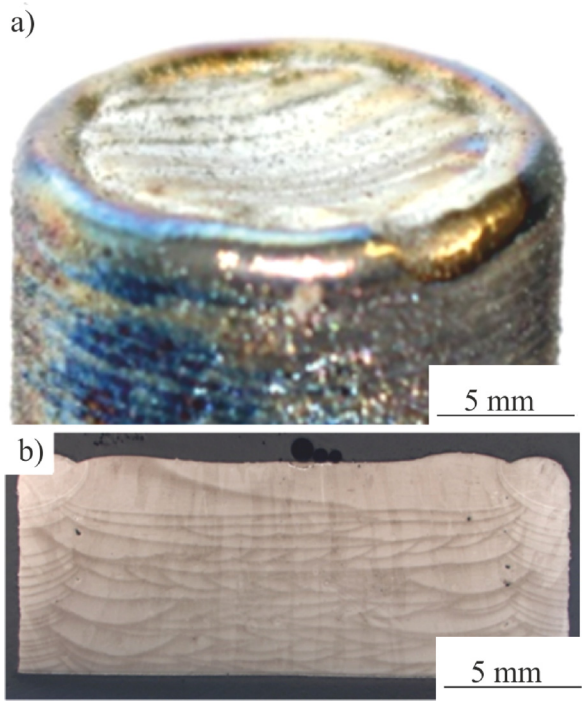

FIG. 5. Experimental results with basic deposition strategy and local shielding gas atmosphere; (a) geometric error; (b) Microstructure (Weck etching).

is applied to ensure an adequate protection of the endpoints by the powder nozzle. The gas delay times from E5c are applied (2 s for endpoint of the circles, 6 s for endpoint pendulum area).

As described in the section "Cylinder build-up with basic deposition strategy and compensation layers," round tensile specimens are machined and tested. X-ray testing is applied to prove the quality of the tensile specimens. After the tensile test, the fractured surfaces are examined via SEM.

IV. RESULTS AND DISCUSSION

A. Cylinder build-up with basic deposition strategy and compensation layers

Figure 5(a) shows the sag in the middle of the pendulum area which occurs after every eight standard layers. It is possible to compensate this sag with the small pendulum square, suggested in Ref. 25. The LMD deposition strategy is clearly visible in the microstructure (Fig. 5(b)). Along the contour, single weld beads are placed on top of each other for good net shape. In the bulk material, the weld beads are placed next to each other with perpendicular direction each layer. The weld beads oriented transversal to the cross section are visible as halfcircles, while in the following layer the weld bead appears as elongated structures. The compensation layer is recognizable in the microstructure and well bonded to the surrounding material. Some pores are visible between the contour tracks and core pendulum strategy. In this case, the contour tracks are only needed to achieve a good net-shape deposition, so no further adjustment is necessary to reduce porosity in this area.

The contour area displays blue and golden heat tint. This is due to the local shielding gas atmosphere. Furthermore,

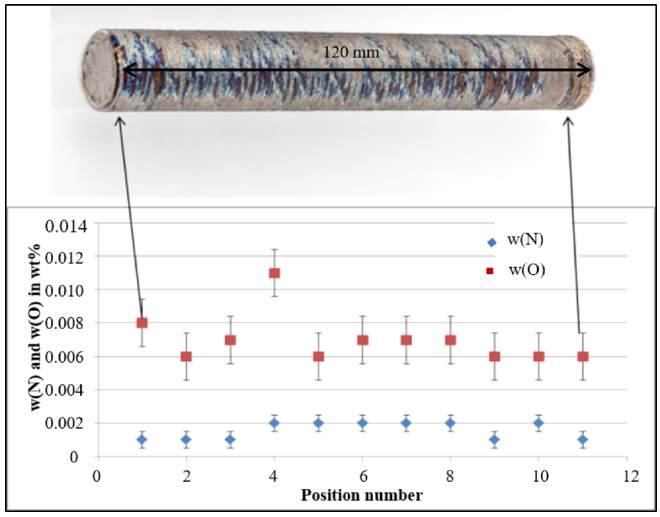

FIG. 6. Results of the gas phase extraction.

the specimen geometry was specifically chosen to create issues with heat accumulation. This shows the need to adjust the deposition strategy, which is described in experimental series E5.

The results of the gas phase extraction tests can be seen in Fig. 6. Average contents of oxygen and nitrogen are in the range of 0.006 wt. %–0.012 wt. %. In comparison to the threshold values for $O < 0.2\%$ and $N < 0.05\%$ given in ASTM F1472 for rolled Ti-6Al-4 V, the global contents in the additive manufactured parts are uncritical and the local shielding gas atmosphere should be suitable. Tensile strength values are within a range of 780 MPa $<$ Rm $<$ 1068 MPa. Fracture strain values are within a range of $0.1\% < A < 1.9\%$. The large spread of the tensile strength values and the low fracture strains show that the build-up strategy in E1 does not lead to reproducible mechanical properties.

To investigate the fracture mechanisms, SEM and EDX analysis of the fractured surfaces are conducted. Two failure mechanisms can be distinguished:

- Failure due to local oxygen enrichment.
- Failure due to incomplete fusion zones.

In Fig. 7(b), the fracture surface of a tensile specimen with local oxygen enrichment can be seen. This surface can be divided into a ductile zone (surface Fig. 7(c)) and a brittle zone (surface Fig. 7(a)). The EDX analysis shows a high oxygen content up to 4 wt. % in the brittle zone and a low oxygen content $\ll$0.5 wt. % in the ductile zone, see Table VI. Therefore, the brittle fracture behavior can be addressed to the partial oxygen enrichment through a locally insufficient shielding gas protection if no gas delay times are applied to prevent the formation of heat tint at the endpoints of a deposited pendulum track.

In Figs. 7(d)–7(f), SEM images of the fracture surface with an incomplete fusion zone are shown. This surface can be divided into two zones. The zone in Fig. 7(d) shows the incomplete fusion zone, while Fig. 7(f) shows the typical microvoid fracture area of a ductile failure. The oxygen content is in both zones $<$0.5 wt. %, see Table VI. In this case, the fracture cause can be addressed to the incomplete fusion

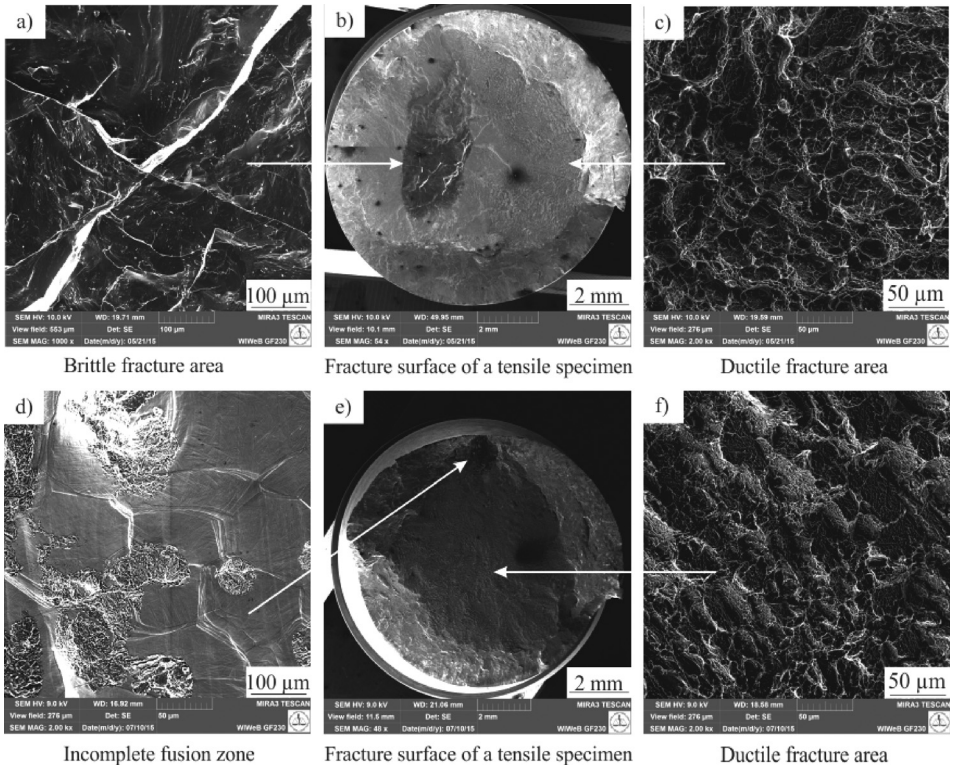

FIG. 7. SEM image of two different fractured surfaces.

zone, located at the start or endpoint of the compensation square.

Originating from the SEM and EDX results different requirements for an improved build-up strategy can be deducted:

- Compensation layers should be avoided.
- All start and endpoints should be placed in contour areas of the parts.
- Longer gas delay times are necessary to improve the shielding gas atmosphere on the endpoint of the compensation layer.
- Global oxygen and nitrogen contents do not allow any conclusions regarding fracture behavior.

B. Improved build-up strategies

1. Avoiding compensation layers with adjusted travel paths and determination of the sag origin in E1

In the experimental series E2 adjoining lines were used to fill the core area. After deposition of 16 layers on every of the four test cylinder, no sag occurs at any time, see Figs. 8(a) and 8(b). Therefore, the sag formation in E1 can be clearly addressed to the pendulum strategy. Due to the position and rotation of the pendulum turning points, multiple track overlaps with the two shell circles occur. This leads to higher deposition rates on the edges and a symmetrical build-up in the shell near areas, see Fig. 9. Additionally, possible changes in the scanning velocity/accuracy at turning points could contribute to the irregularities, see Refs. 27 and 41. It is important to note that the laser power is adjusted according to the changed velocity at turning points, leading to a constant energy input per unit length. In consideration of the track overlap ratios shown in Fig. 9, it can be seen that the overlap ratios are not uniform at the start- and endpoints (triangle shaped travel paths) due to the desired cylinder geometry. These changing overlap ratios (from 100% overlap to 50% overlap) should contribute to the sag formation, according to the mechanisms described in Refs. 23–25. Relating to these insights, it would be more precise to call the geometrical error "shell near superelevation" instead of sag.

Although the application of adjoining weld beads in E2 seems promising to fill the cylinder inlets without any sag formation, the layers show major geometrical errors at the start points. This is caused due to a lower deposition rate when the molten pool is in formation.

TABLE VI. Results of the EDX analysis.

	Failure due to oxygen enrichment	
Element	Brittle zone 7 a)	Ductile zone 7 c)
Ti	Rest	Rest
Al	5 wt. %–6 wt. %	4 wt. %–5 wt. %
V	3 wt. %–4 wt. %	4 wt. %–5 wt. %
O	3 wt. %–4 wt. %	≪0.5 wt. %
Failure due to incomplete fusion zones		
Element	Incomplete fusion zone 7 d)	Ductile area 7 f)
Ti	Rest	Rest
Al	4 wt. %–5 wt. %	4 wt. %–5 wt. %
V	4 wt. %–5 wt. %	4 wt%–5 wt. %
O	<0.5 wt. %	≪0.5 wt. %

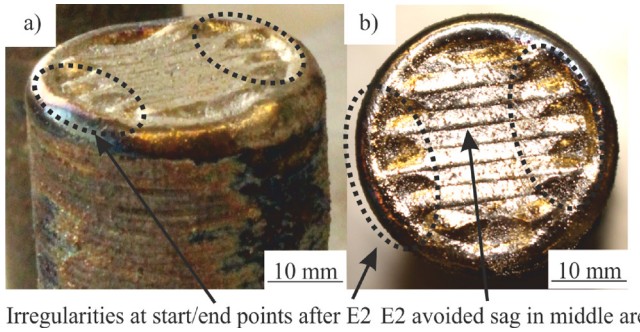

FIG. 8. Experimental results of the single line deposition E2; (a) side view; (b) top view.

In consideration of this, the following conclusion can be made:

An adjusted pendulum strategy should be applied to avoid the sag formation as well as irregularities at starting points.

2. Avoiding compensation layers with variable track overlap

Variable track overlap ratios are applied in E3 and E4 to compensate the sag (negative hemisphere profile) within a standard pendulum layer. The overlap ratios in experimental series E3 lead to a positive hemisphere profile. This indicates that the overlap ratios of the inner layers are oversized. In contrast the overlap ratios in E4 lead to an all-time even surface independently of the number of layers. Some selected results are shown in Fig. 10.

The following improvements toward E1 can be summarized:

According to the results from the SEM analysis in E1, start- and endpoints within the final component geometry (in this case the tensile test specimen) should be avoided due to a possible formation of incomplete fusion zones, as shown in Figs. 7(d)–7(f). This is achieved by the application of variable overlap ratios. Strategy E4 is capable to generate flat cylinder surfaces without the application of compensation layers. Consequently, no start- and endpoints are placed in the final geometry and the build-up process is well automatable due to an even layer height. The same applies for more complex 3D geometries, where the start- and endpoints of layers could be placed outside the target geometry (after postprocessing) whenever possible, and varying overlap ratios could help in the creation of even layers.

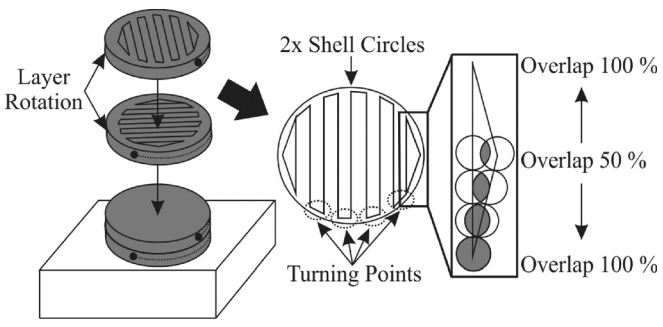

FIG. 9. Sag formation in E1 due to turning points and variable track overlap.

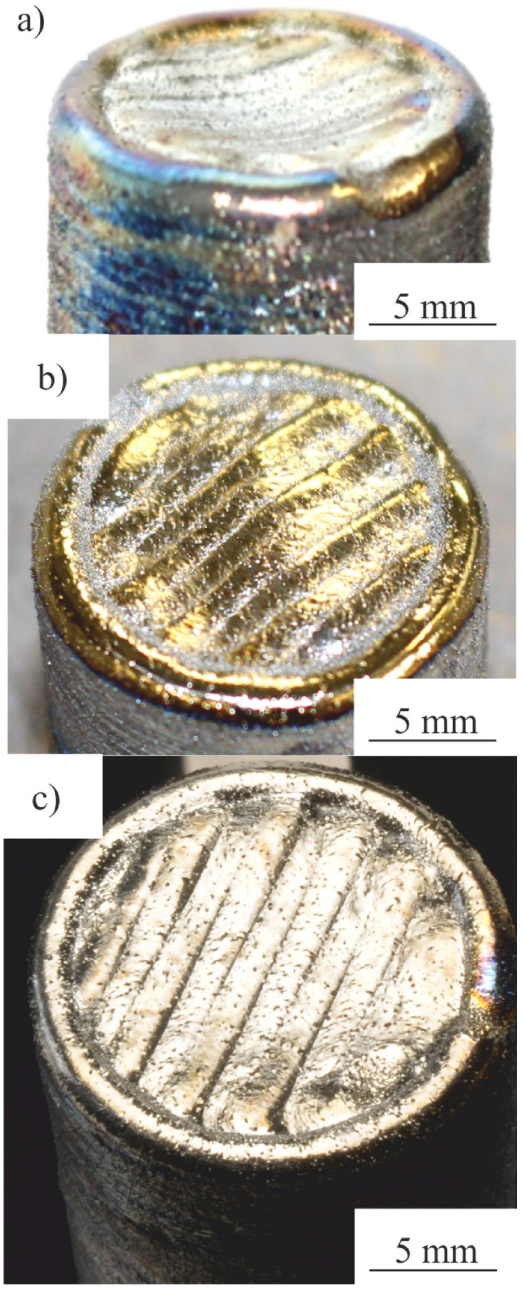

FIG. 10. Variable track overlap; (a) E1, negative surface profile; (b) E3, positive surface profile; (c) E4, flat surface.

3. Optimization of the cooling conditions

The occurrence of heat tint depends on three main effects:

- The cylinder height h (at constant cylinder diameter).
- The interlayer cooling period t_c between two superimposed layers.
- The gas delay time at heated endpoints.

With short cooling periods ($t_c = 17.5$ s), no heat tint can be seen for the deposition of the first three superimposed layers directly on the substrate plate (Fig. 11(a)). In this area, the heat dissipation in the substrate is high as shown by the results of the pyrometer and thermographic camera measurements in Figs. 13 and 14. The black curves in Fig. 13 show the cooling behavior of the pendulum endpoint between

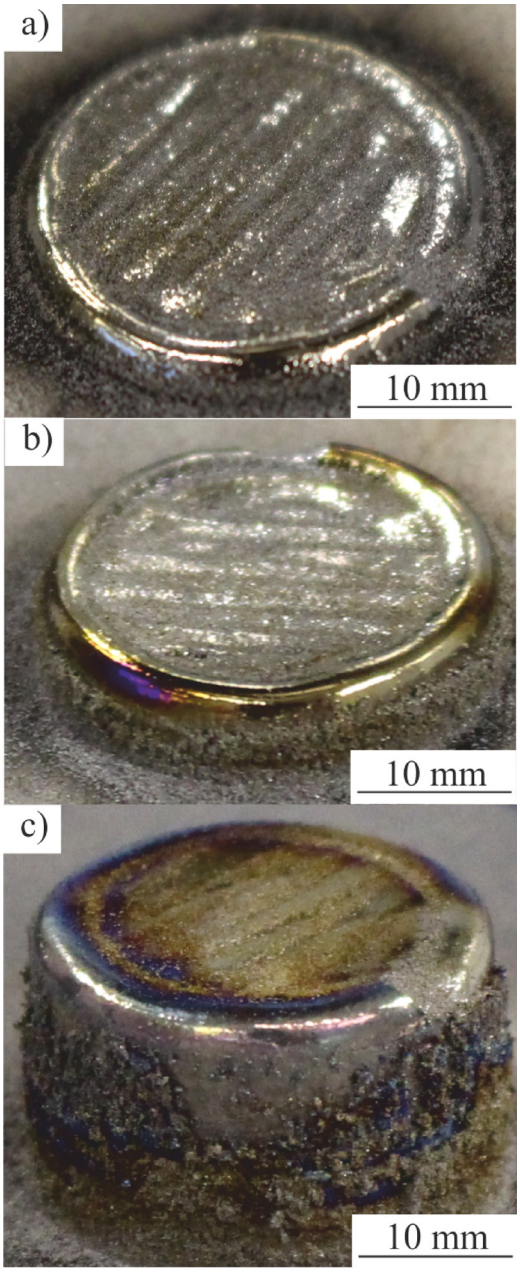

FIG. 11. Heat tint as a function of the cylinder height in E5a; (a) 1.5 mm (3 layers); (b) 3 mm (6 layers); (c) 15 mm (30 layers).

950 °C and 400 °C for the deposition of three consecutive layers directly on the (cold) substrate plate. It can be seen that the cooling times are slightly prolonged at the endpoint of about 1.5 s per layer.

The thermographic measurements in Fig. 14 indicate the fast cooling cycle below 300 °C of the whole cylinder surface after the deposition. For the following superimposed layers (4–6) heat tint starts to occur at the shell. This effect can be addressed to the lower heat dissipation along the shell. Furthermore, the shielding gas stream is not uniform on the edges. Once the cylinder height reaches around 15 mm (~30 layers) the heat tint is also observable on the core surface. Selected results of E5a are portrayed in Figs. 11(a)–11(c). Therefore, the cylinder height has to be taken into account. By an increasing height, the heat dissipation decreases until the heat exchange reaches a quasisteady state for constant cooling conditions.[14] The gray curves in Fig. 13 show the transient temperature behavior of the same three consecutive layers deposited on a (cold) cylinder in a height of 100 mm. The difference between deposition on the substrate plate or on the cylinder is clearly visible. The temperature curve T(t) of layer 1 on the cold substrate plate reaches a temperature of 400 °C after less than 3.5 s. In contrast, the curve T(t) layer 1 on the cold cylinder has a temperature of more than 550 °C at that time. Far from the substrate the heat dissipation is smaller, resulting in significant slower cooling speed of the whole cylinder surface and the endpoint of the pendulum area in particular, see Fig. 14. Therefore, the test results on a cylinder height of 100 mm show varying magnitudes of heat tint, depended on the applied cooling periods.

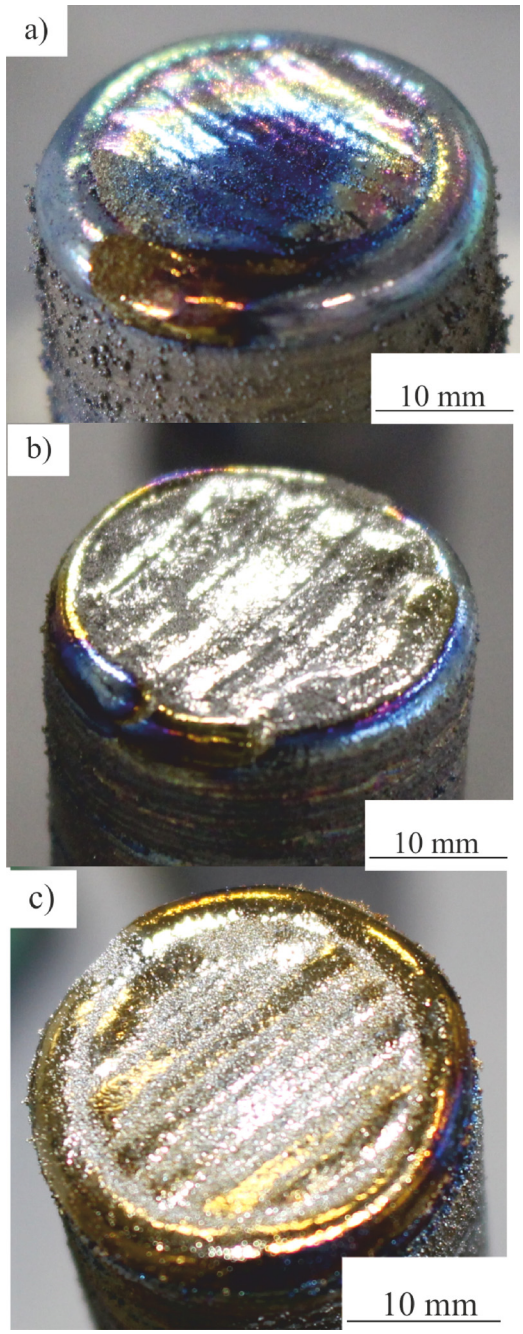

FIG. 12. Heat tint as a function of the cooling period E5b; (a) $t_c = 17.5$ s; (b) $t_c = 62.5$ s; (c) $t_c = 126$ s.

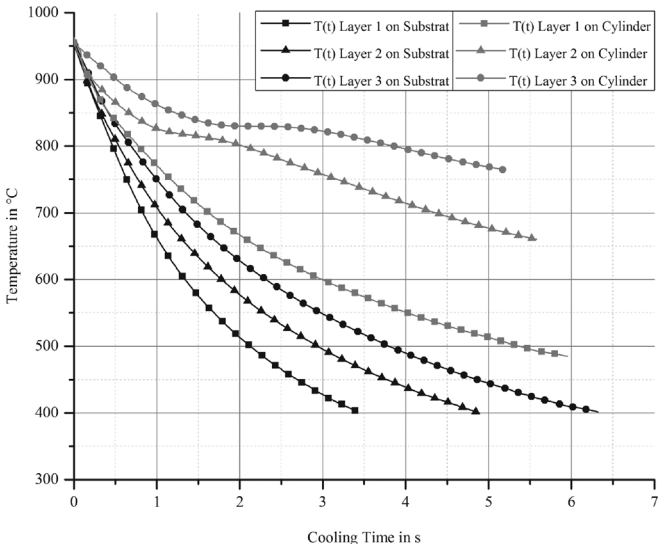

FIG. 13. Cooling behavior between 950 °C and 400 °C, depending on the build-up height and number of layers, two-color pyrometer, measurement on the layer surface (end-point of the deposition).

Selected results of E5b are portrayed in Figs. 12(a)–12(c). It can be seen that the heat tint decreases by an increased cooling period. With a cooling period of $t_c \geq 100$ s almost blank layers arise. The observations during experimental series E5b show that an adequate cooling period is also important to reach a constant layer height. If cooling periods are too short the layer height will decrease during the ongoing deposition. For instance, with 29 layers and a cooling period of 17.5 s per layer, an increment of cylinder height of 12.1 mm is reached. That is 2.4 mm below the expected increase of 14.5 mm. This effect, which is probably caused by an overheating and track widening, is described by Ocylok *et al.* in Ref. 42 and has to be avoided for an automated build-up process. If there is no control loop to keep the surface-nozzle distance at a constant value, the nozzle distance would increase and process stability would be further deteriorated.

Because the endpoints of a deposited track are exposed to the highest temperatures due to heat accumulation effects (see Fig. 13 and Ref. 19) and are the latest heated points in the deposition cycle as well, a gas delay time is applied in E5c. Within the gas delay time the heated endpoints are shielded by the gas stream provided by the nonmoving powder nozzle. It was found that the endpoints of the pendulum area are free of heat tint when a gas delay time of 6 s is applied. In comparison to the results of the pyrometer and thermographic camera measurements a gas delay time of 6 s is sufficient to cool the deposit below a critical temperature due to consecutive gas flow. Because the deposited shell circles do not belong to the final geometry, just a gas delay of 2 s is adjusted to avoid a strong heat tint.

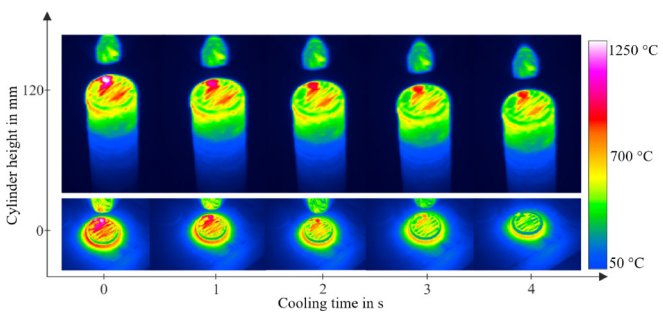

FIG. 14. Thermographic camera measurements (images corrected by emissivity to get temperatures): cooling behavior after pendulum deposition on substrate and cylinder.

The temperature measurements in E5 are in good agreement to the expected general behavior based on the simulations discussed in the state of the art.[28,29] The heat accumulation is visible, leading to different heat tint depending on the cylinder height. As shown in Refs. 30–32, a monitoring and control system would be one option to deal with this issue. Since the complexity and investment cost of these systems are high, they are best suited for high-tech applications like turbine blades. For small- and medium sized industrial operators like job- shops, systems with less complexity might be useful. This includes the approach followed in experimental series E1-E5, where issues with heat accumulation are dealt with by the design of the deposition strategy.

The results of experimental series E5 show once again the relevance and the difficulties when only a local shielding gas protection is applied and parts with low heat deduction are built. By the consideration of the build-up height, heat tint free surfaces can be obtained when the interlayer cooling periods as well as the gas delay times are adjusted. For the cylinder build-up with local shielding gas protection the following improvements toward E1 can be summarized:

According to the results from the melt extraction tests in E1, the local shielding gas protection provided by the powder nozzle is sufficient to ensure a low global content of atmospheric gases if the interlayer cooling periods are sufficient high. This constraint is reached for the automatized build-up process in E5b due to the applied interlayer cooling period of t_c 126 s. Even if the global content of atmospheric gases is below the global standard values, local oxygen enrichments can lead to a premature failure as the results of the EDX analysis in Fig. 7(a) show. Due to included gas delay times of 6 s at the endpoints of the pendulum area E5c is capable to deal with this issue.

C. Cylinder build-up with variable track overlap ratios and optimized cooling conditions

In this part of the investigations, the optimized build-up process is performed with the pendulum strategy shown in E4 and an interlayer cooling period of 126 s (E5b). For single component manufacturing, this would lead to prolonged manufacturing times. However, five cylinders are manufactured at the same time, so the deposition process is continued on the next cylinder during the cooling period of the previous cylinder. Additionally, the inert gas delay times determined in E5c are applied. Because the contour track is not part of the final tensile specimen, just a minimum gas delay of 2 s is required to avoid a strong heat tint. After every core deposition, the inert gas delay is set to 6 s. No compensation layer (square) is needed due to the variable track overlaps designed for E4. In total 240 layers are necessary to build each of the 123 mm high cylinders shown in Fig. 15(a). The deposition time ("laser on") amounts to 6.7 h for five

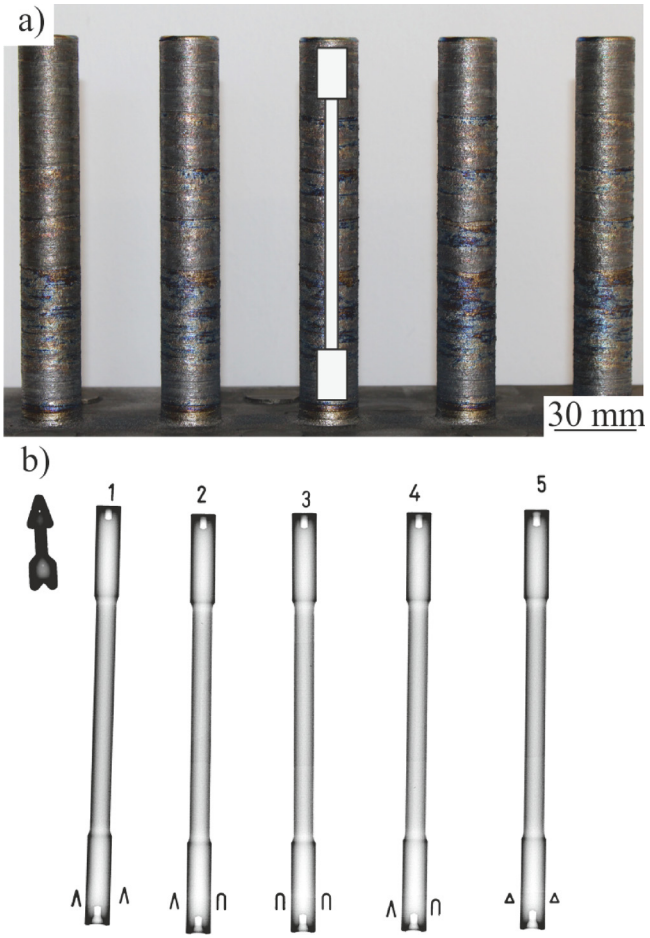

FIG. 15. (a) 123 mm high blanks; (b) X-ray analysis of the tensile specimen.

cylinders, while the overall manufacturing time (including gas delay time and traverse paths) is 11.3 h. The powder efficiency is 59.4%.

The X-Ray analysis shows no defects within the machined tensile specimens, see Fig. 15(b). With a tensile strength of 923 MPa ± 9 MPa and a yield strength of 876 MPa ± 6 MPa, the mechanical properties of the specimen range between the given standard values of ASTM F1108 and ASTM F1472, see Table I. In comparison to the LMD properties given in Table I, the yield and tensile strength values in these experiments are quite good when the challenging build-up conditions are considered. Furthermore, the good material quality results in a high value of 10.1% ± 1.5% for the fracture strain. This finding is supported by the microscopic examination of the fracture surface, see Fig. 16. The dimple structure confirms the ductile fracture behavior and therefore the suitability of the applied strategies.

V. SUMMARY AND CONCLUSIONS

In order to adjust the build-up strategy and to deposit material on existing parts with complex shape for an additive LMD process, a high flexibility in the movement of the powder nozzle is necessary. This flexibility is achieved as long as the shielding gas atmosphere is created only by a coaxial LMD powder nozzle. In this case, issues with the restricted size and quality of the local shielding gas atmosphere arise,

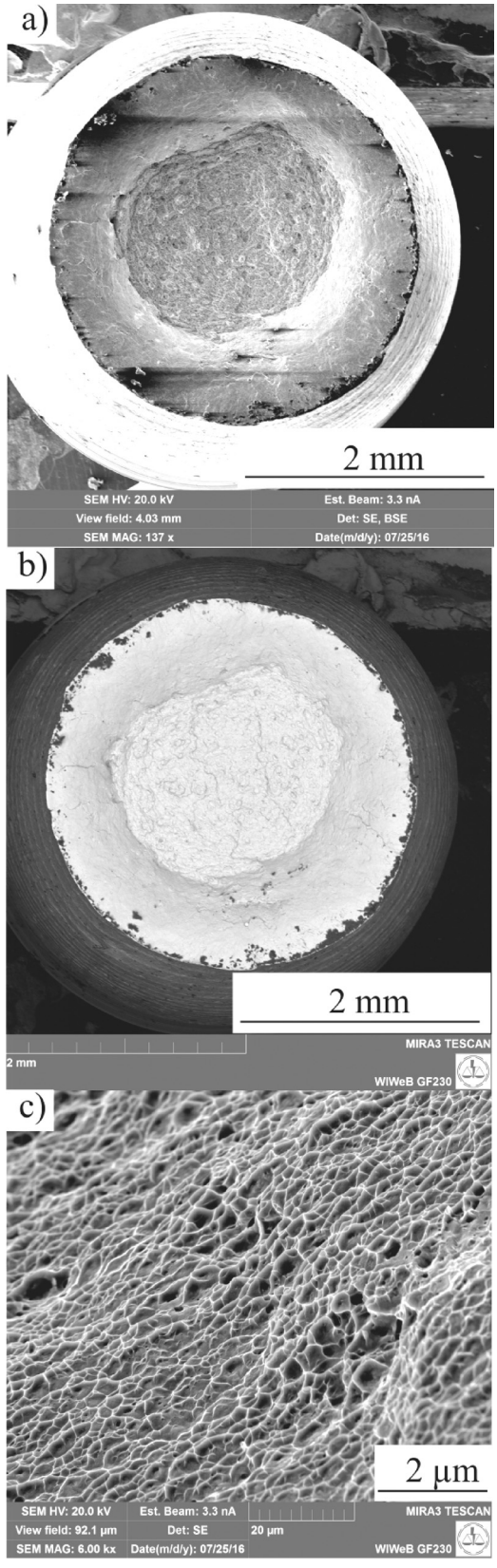

FIG. 16. SEM images of the fractured surfaces using optimized build-up strategies; (a) cup; (b) cone; (c) microvoid surface.

especially when titanium alloys are processed and the heat dissipation is poor.

In the experiments, lean cylinders with a height of 123 mm and a diameter of approximately 19 mm are

manufactured as blanks for round tensile specimens. These near net shape parts with perpendicular edges can be processed in arbitrary height using a core/shell strategy consisting of two contour circles and an inner pendulum strategy. To avoid compensation layers pendulum strategies with variable track overlap ratios are successfully used to adjust the layer height. Transferring this new strategy to other basic shapes like cuboids, lower deposition rates in edge areas could be compensated without the need for error-prone compensation strategies. Furthermore, whenever a desired shape requires travel paths with unstable track overlap ratio, variable track overlaps can be used to compensate fluctuations in the geometry. In combination with adjusted gas delay times and sufficient interlayer cooling periods, multiple specimens can be built efficiently within one batch. The tensile tests prove good strength values of 923 ± 9 MPa for the presented build-up strategies. Besides this, good strain values in the range of $10.1\% \pm 1.5\%$ are achieved.

The results impressively show that Ti-6Al-4 V can be processed to near net shape specimens with high aspect ratios with a single LMD process nozzle. Tensile strength and strain values comparable to wrought Ti- 6Al-4 V material specifications can be achieved without any subsequent heat treatment, when:

- A sound build-up strategy is applied.
- Interlayer cooling periods between single layers are sufficient and gas delay times are applied.
- All start and endpoints are placed in contour areas of the parts.

With customized track overlap ratios and gas flow times, additional trailing nozzles or process chambers are not mandatory for LMD additive manufacturing of titanium alloys. Therefore, the LMD-process is able to make a contribution to an efficient machining of "difficult to cut" materials like titanium alloys.

[1]European_Commission, "Flightpath 2050," 2011.
[2]E. Uhlmann, R. Kersting, T. B. Klein, M. F. Cruz, and A. V. Borille, "Additive manufacturing of titanium alloy for aircraft components," Procedia CIRP **35**, 55–60 (2015).
[3]C. Leyens and M. Peters, *Titanium and Titanium Alloys: Fundamentals and Applications* (WILEY-VCH, 2003).
[4]F. Klocke, A. Klink, D. Veselovac, D. K. Aspinwall, S. L. Soo, M. Schmidt, J. Schilp, G. Levy, and J. P. Kruth, "Turbomachinery component manufacture by application of electrochemical, electro-physical and photonic processes," CIRP Ann. Manuf. Technol. **63**(2), 703–726 (2014).
[5]K. G. Hänsel and K. L. Schiff, "Laser beam welding of refractory metals," in *Laser Treatment of Materials* (Oberursel, DE, 1987), pp. 341–348.
[6]B. Wu, D. Ding, Z. Pan, D. Cuiuri, H. Li, J. Han, and Z. Fei, "Effects of heat accumulation on the arc characteristics and metal transfer behavior in wire arc additive manufacturing of Ti6Al4V," J. Mater. Process. Technol. **250**(C), 304–312 (2017).
[7]G. Zhu, A. Zhang, D. Li, Y. Tang, Z. Tong, and Q. Lu, "Numerical simulation of thermal behavior during laser direct metal deposition," Int. J. Adv. Manuf. Technol. **55**(9), 945–954 (2011).
[8]A. Gasser, J. Witzel, and M. Goebel, "Additive manufacturing of turbo-engines applications," in *ICTM conference*, 2013.
[9]E. Brandl, B. Baufeld, C. Leyens, and R. Gault, "Additive manufactured Ti-6Al-4V using welding wire: comparison of laser and arc beam deposition and evaluation with respect of aerospace material specifications," LANE, Phys. Procedia **5**, 595–606 (2010).
[10]F. Wang, J. Mei, H. Jiang, and X. Wu, "Laser fabrication of Ti6Al4V/TiC composites using simultaneous powder and wire feed," Mater. Sci. Eng. A **445–446**, 461–466 (2007).
[11]C. Qiu, G. A. Ravi, C. Dance, A. Ranson, S. Dilworth, and M. M. Attallah, "Fabrication of large Ti-6Al-4V structures by direct laser deposition," J. Alloys Compd. **629**, 351–361 (2015).
[12]J. Yu, M. Rombouts, G. Maes, and F. Motmans, "Material properties of Ti6Al4V parts produced by laser metal deposition," Phys. Procedia **39**, 416–424 (2012).
[13]J. Yao, T. Suo, S. Zhang, F. Zhao, H. Wang, J. Liu, Y. Chen, and Y. Li, "Influence of heattreatment on the dynamic behavior of 3D laserdeposited Ti–6Al–4V alloy," Mater. Sci. Eng. A **677**, 153–162 (2016).
[14]R. Bi, G. Gasser, A. Wissenbach, K. Drenker, and A. Poprawe, "Characterization of the process control for the direct laser metallic powder deposition," Surf. Coat. Technol. **201**, 2676–2683 (2006).
[15]A. Candel-Ruiz, S. Kaufmann, and O. Müllerschön, "Strategies for high deposition rate additive manufacturing by laser metal deposition," in *Lasers in Manufacturing Conference* (2015), no. 0, pp. 2–7.
[16]X. Wu and J. Mei, "Near net shape manufacturing of components using direct laser fabrication technology," J. Mater. Process. Technol. **135**(2–3), 266–270 (2003).
[17]M. Hedges and N. Calder, "Near net shape rapid manufacture & repair by LENS," in *Cost Eff. Manuf. via Net-Shape Process, Meet. Proc. RTO-MP-AVT-139* (2006), vol. 2, p. 13.
[18]B. Graf, A. Gumenyuk, and M. Rethmeier, "Laser metal deposition as repair technology for stainless steel and titanium alloys," Phys. Procedia **39**, 376–381 (2012).
[19]J. N. Montero, A. Rodríguez, J. M. Amado, M. J. Tobar, and A. Yáñez, "Some optimization strategies for tool path generation in 3D laser metal deposition," *Lasers Manufacturing Conference*, 2015.
[20]E. Uhlmann, M. Rethmeier, B. Graf, R. Kersting, and A. Bergmann, "Flexible manufacturing with an additive process chain: Design, production and surface finish," in *ASPE 2015 Spring Topical Meeting: Achieving Precision Tolerances in Additive Manufacturing* (2015), p. 5.
[21]A. J. Pinkerton, "Advances in the modeling of laser direct metal deposition," J. Laser Appl. **27**, S15001 (2015).
[22]B. Graf, S. Ammer, A. Gumenyuk, and M. Rethmeier, "Design of experiments for laser metal deposition in maintenance, repair and overhaul applications," Procedia CIRP **11**, 245–248 (2013).
[23]K. Zhang, W. Liu, and X. Shang, "Research on the processing experiments of laser metal deposition shaping," Opt. Laser Technol. **39**(3), 549–557 (2007).
[24]S. Kaierle, A. Barroi, C. Noelke, J. Hermsdorf, L. Overmeyer, and H. Haferkamp, "Review on laser deposition welding: From micro to macro," Phys. Procedia **39**, 336–345 (2012).
[25]T. Petrat, B. Graf, A. Gumenyuk, and M. Rethmeier, "Build-up strategies for generating components of cylindrical shape with laser metal deposition," *Lasers Manufacturing Conference* (2015).
[26]D. M. Hensinger, A. L. Ames, and J. L. Kuhlmann, "Motion planning for a direct metal deposition rapid prototyping system," *Proc. 2000 ICRA* (2000), pp. 3095–3100.
[27]Y. M. Zhang, Y. Chen, P. Li, and A. T. Male, "Weld deposition-based rapid prototyping: A preliminary study," J. Mater. Process. Technol. **135**(2–3), 347–357 (2003).
[28]K. Zhang, S. Wang, W. Liu, and R. Long, "Effects of substrate preheating on the thin-wall part built by laser metal deposition shaping," Appl. Surf. Sci. **317**, 839–855 (2014).
[29]P. Peyre, P. Aubry, R. Fabbro, R. Neveu, and A. Longuet, "Analytical and numerical modelling of the direct metal deposition laser process," J. Phys. D Appl. Phys. **41**, 1–10 (2008).
[30]S. K. Everton, M. Hirsch, P. Stravroulakis, R. K. Leach, and A. T. Clare, "Review of in-situ process monitoring and in-situ metrology for metal additive manufacturing," Mater. Des. **95**, 431–445 (2016).
[31]L. Tang and R. G. Landers, "Melt pool temperature control for laser metal deposition processes—Part I: Online temperature control," J. Manuf. Sci. Eng. **132**(1), 11010–11019 (2010).
[32]L. Song, V. Bagavath-Singh, B. Dutta, and J. Mazumder, "Control of melt pool temperature and deposition height during direct metal deposition process," Int. J. Adv. Manuf. Technol. **58**(1–4), 247–256 (2012).
[33]X. Wu, J. Liang, J. Mei, C. Mitchell, P. S. Goodwin, and W. Voice, "Microstructures of laser-deposited Ti-6Al-4V," Mater. Des. **25**(2), 137–144 (2004).

[34]E. Brandl, V. Michailov, B. Viehweger, and C. Leyens, "Deposition of Ti-6Al-4V using laser and wire, part I: Microstructural properties of single beads," Surf. Coatings Technol. **206**(6), 1120–1129 (2011).
[35]R. Raju, M. Duraiselvam, V. Petley, S. Verma, and R. Rajendran, "Microstructural and mechanical characterization of Ti6Al4V refurbished parts obtained by laser metal deposition," Mater. Sci. Eng. A **643**, 64–71 (2015).
[36]B. E. Carroll, T. A. Palmer, and A. M. Beese, "Anisotropic tensile behavior of Ti-6Al-4V components fabricated with directed energy deposition additive manufacturing," Acta Mater **87**, 309–320 (2015).
[37]S. H. Mok, G. Bi, J. Folkes, I. Pashby, and J. Segal, "Deposition of Ti-6Al-4V using a high power diode laser and wire, Part II: Investigation on the mechanical properties," Surf. Coatings Technol. **202**(19), 4613–4619 (2008).
[38]P. A. Kobryn and S. L. Semiatin, "Mechanical properties of laser-deposited Ti-6Al-4V," Solid Free. Fabr. Proc. (2001), pp. 6–8.
[39]B. Baufeld, E. Brandl, and O. van der Biest, "Wire based additive layer manufacturing: Comparison of microstructure and mechanical properties of Ti–6Al–4V components fabricated by laser-beam deposition and shaped metal deposition," J. Mater. Process. Technol. **211**(6), 1146–1158 (2011).
[40]A. M. Beese and B. E. Carroll, "Review of mechanical properties of Ti-6Al-4V made by laser-based additive manufacturing using powder feedstock," Jom **68**(3), 724–734 (2016).
[41]D. Boisselier, S. Sankar, and T. Engel, "Improvement of the laser direct metal deposition process in 5-axis configuration," Phys. Procedia **56**(C), 239–249 (2014).
[42]S. Ocylok, E. Alexeev, S. Mann, A. Weisheit, K. Wissenbach, and I. Kelbassa, "Correlations of melt pool geometry and process parameters during laser metal deposition by coaxial process monitoring," Phys. Procedia **56**, 228–238 (2014).

Meet the Authors

Felix Spranger, M. Sc., studied production technology at the Technical University Berlin. His master thesis dealt with build-up strategies for laser metal deposition of titanium for additive manufacturing. He works on the field of laser surface structuring at BAM as Ph.D-student in an interdisciplinary research project combining laser surface engineering and tribology.

Benjamin Graf is head of Department for joining technology at Fraunhofer IPK. His working field comprises laser metal deposition, with its applications in wear protection, repair and additive manufacturing.

Michael Schuch works at the Bundeswehr Research Institute for Materials, Fuels and Lubricants (WIWeB) in Erding. In his scientific work, he specializes on protective materials.

Professor Kai Hilgenberg studied mechanical engineering and wrote his Ph.D. thesis on a laser surface treatment of tool steels at the Chair of Metal Forming Technology at the University of Kassel. Afterward, he worked as postdoc and since 2015 as Junior-Professor at the Technical University of Berlin and at the Federal Institute of Materials Research and Testing in Berlin in the field of laser welding and laser based additive manufacturing.

Professor Rethmeier studied mechanical engineering at the Technical University "Carolo Wilhelmina Braunschweig." He worked as corporate research project manager at Volkswagen from 2002 till 2006, before joining the Federal Institute for Materials Research and Testing, BAM. Professor Rethmeier is leading the division "Joining and Coating Technology" at Fraunhofer IPK in Berlin.